J Mater Sci (2009) 44:2599–2609
DOI 10.1007/s10853-009-3340-z

Refined model of elastic nanoindentation of a half-space by the blunted Berkovich indenter accounting for tangential displacements on the contact surface

Vitaliy M. Kindrachuk · Boris A. Galanov · Valeriy V. Kartuzov · Sergey N. Dub

Received: 20 July 2008 / Accepted: 10 February 2009 / Published online: 9 March 2009

Abstract Elastic contact between a non-ideal Berkovich indenter and a half-space is investigated. The derived mathematical model of the contact allows for tangential displacements of the boundary points of the half-space. The tip of the blunted indenter is simulated as a smooth surface. The boundary element method is implemented in the model for numerical simulation of nanoindentation. The relative deviation function is introduced and calculated to quantify the influence of the tangential displacements on the load–displacement curves. A simple expression is derived for the impact of the tangential displacements on the values of the reduced Young's modulus determined due to nanoindentation studies. The refined model was successfully applied to simulate the experimental load–displacement curves gained by elastic nanoindentations of flat LiF and KCl samples. Such values of the indenter bluntness (the varying parameter) were found that the simulated load–displacement curves coincided with those of the experimental data at displacements higher than 7.5 nm. The model neglecting tangential displacements gives slightly differing values for the parameter of the indenter bluntness.

V. M. Kindrachuk (✉)
Division V.2: Mechanical Behaviour of Materials,
Federal Institute for Material Research and Testing (BAM),
Unter den Eichen 87, Berlin 12205, Germany
e-mail: vitaliy.kindrachuk@bam.de

B. A. Galanov · V. V. Kartuzov
Frantzevich Institute for Problems of Materials Science,
Kyiv 252142, Ukraine

S. N. Dub
Institute for Superhard Materials, Kyiv 04074, Ukraine

List of symbols

O, x_1, x_2, x_3	Cartesian coordinate system
M, N	Points on the plane $x_3 = 0$
R_{MN}	Distance between points $M(x_1, x_2)$ and $N(\xi, \eta)$
r	Distance between point M and the origin O, $r = \sqrt{x_1^2 + x_2^2}$
h	Displacement of the indenter
$f(x_1, x_2)$	Gap between the indenter and the specimen before deformation
γ	Angle between Ox_3 and $O'E$, depends on the position of M (see Fig. 1)
R	Radius describing the shape of the blunted indenter tip, depends on the position of M
β	Indenter parameter, $\beta = \cot 65.3^\circ = 0.46$
d	Bluntness of the indenter tip
r_c	Distance between the origin O and the contour of the orthogonal projection of the bluntness to the plane $x_3 = 0$
S	Orthogonal projection of the contact region on the plane $x_3 = 0$ after deformation
Ω	An arbitrary area in the plane $x_3 = 0$ containing the contact region
$v(M),\ M \in \Omega$	Unknown function in the integral boundary equation
P	Force applied to the indenter in the direction normal to the flat surface of the specimen
$P_0(h)$	Dimensionless compression force
E_i, υ_i	Young's modulus and Poisson's ratio respectively of the diamond indenter
E_s, υ_s	Young's modulus and Poisson's ratio respectively of the sample
$K(M, N)$	Kernel of the integral operator
ε	$\varepsilon = \frac{1}{2} \cdot \frac{1-2\upsilon_s}{1-\upsilon_s}$

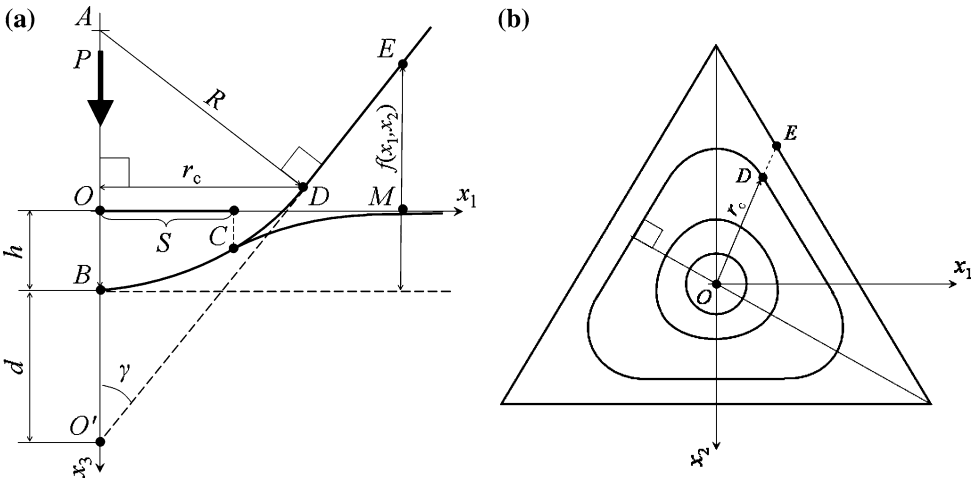

Fig. 1 **a** Geometry of the simulated blunted indenter, *BCDE*, and of the ideal Berkovich indenter, *O′DE*. The segment *BD* is the arc of the circle with the centre *A* and radius *R*; *d* is the bluntness of the indenter tip. *OB* is the displacement of the indenter, which causes the contact *BC* with the sample. **b** Cross-section of the simulated blunted indenter. The contour lines correspond to various positions of *D*

Introduction

Indentation is a widely used tool in the study of mechanical properties of materials, such as hardness *H* and elastic modulus *E* on the micro- and millimeter scales. For the analysis of material on the smaller scale a nanoindentation technique has been developed. However, the results gained by the nanoindentation test are more complicated to interpret. A number of factors have to be taken into account, since they are highly relevant on the nanometer scale. These can be the roughness of contacting surfaces, non-planar surface of samples, non-ideal shape of indenters, etc. Therefore, a more careful examination of exactly what these effects cause on the interpretation of nanoindentation is required.

In respect to development of its mathematical model, indentation is a subject of the contact mechanics. Hertz [1] presented the first theory of mechanical contact more than a century ago. It is restricted to frictionless contact between elastic bodies and smooth surfaces. Hertz considered only the normal displacements on the surface of solids. However, it is known [2, 3] that the Hertzian formulation of the contact problem causes incompatibility of strains in the area around the contact. It was shown in [2] that the mentioned incompatibility of strains depends strongly on whether the formulation of the contact problem takes into account the free tangential displacements on the contact surfaces. Thus, eliminating the tangential displacements leads to an approximate solution which possesses the specified unnatural property. Therefore, accounting for the tangential displacements demands a particular investigation.

A two-dimensional (2D) elastic contact problem in a refined formulation was studied analytically in different works [4–7]. Brock considered self-similar elasto-dynamic indentations of a half-plane by a rigid wedge [4]. Similar to Brock, Georgiadis investigated a static indentation of an elastic half-plane by a rigid wedge [5]. Both authors concluded that a singularity in the contact stress at the wedge apex did not occur after accounting for tangential displacements. However, the boundary integral equation method was suggested for more general and difficult contact problems [5]. Soldatenkov derived a more common solution supposing a rigid symmetric punch [6, 7]. Anyway, the solution of three-dimensional (3D) contact problems is in general more difficult than the solution of 2D problems, because no single mathematical apparatus analogous to the theory of functions of a complex variable in the 2D case exists for handling 3D problems. Thus, 3D problems require a special approach and the application of new mathematical tools.

The tangential displacements in the 3D elastic contact problem were firstly accounted for in the works of Galanov [2, 8] and later in the works of Argatov [9, 10]. Argatov gave a closed-form approximate solution for a contact of a punch shaped like a paraboloid of revolution. Galanov obtained numerical solutions for the contact of a punch shaped like a regular square pyramid, like a cone or like a paraboloid of revolution. He found out that the value of the tangential displacements at the boundary of the contact region could achieve approximately 22% of the indentation depth depending on the Poisson's ratio of the elastic half-space. The incompatibility of strains in the area around the contact was observed in each case.

Galanov investigated ideal indenters in his studies. We would consider indenters having some deviations from their nominal shapes, like the blunted tips. The allowance for the bluntness of the indenter tip leads to a more precise formulation of the contact problem, because the deviation of the indenter tip from its nominal geometry is known to be the most significant source of uncertainty in nanoindentation measurements [11]. Some uncertainties in nanoindentation measurements, which are sometimes attributed to properties of the material, can be explained and quantitatively described by properly accounting for geometric deviation of the indenter tip [12]. So, the

approach used by Galanov in [2, 3, 8] is applied in the present work to solve the refined 3D contact problem, which accounts for both the tangential displacements on the contact surface and for the bluntness of the indenter tip. The model derived in the paper concerns an especially important case of shallow indentation (usually less than 100 nm) where the tip bluntness is on the same order as the indentation depth. We consider the indentation of half-spaced samples by the widely used Berkovich indenter. A rigid indenter (a punch) is assumed. Therefore, there are elastic tangential displacements only on the surface of the sample. The other hypotheses of the Hertzian formulation remain without changes. The method of non-linear integral boundary equations (NIBEs) is applied to formulate the problem [13, 14]. The numerical solution of NIBEs is carried out by means of the boundary element method.

The analysis of nanoindentation by an ideal Berkovich indenter or by the bluntness of a non-ideal Berkovich indenter is a complicated problem itself, since the axi-symmetric Galin–Sneddon solution is invalid in this case [15]. However, fundamental relations for general 3D schemes of nanoindentation by indenters of non-ideal shapes were derived [12], where the indenter shape near the tip was approximated by homogeneous functions. It was shown, that degrees of the shape functions for blunted indenters vary between 1 (cone or pyramid) and 2 (elliptic paraboloid tip). Therefore, an approximation of the indenter bluntness by the homogeneous functions with the degree 2 is used in the present study, in order to derive a numerical solution for the load–displacement curves of nanoindentation.

The mathematical model presented in this work is formulated in a dimensionless form. This has two advantages. First, the model is valid both for elastic micro- and macro-contacts. Second, the simulation of nanoindentation data becomes more convenient, since the results of numerical solutions of the dimensionless problem can be easily rescaled to match conditions of a real experiment.

The influence of tangential displacements on the load-displacement curves is theoretically investigated in the first part of the paper. The refined model is verified in the second part, where the bluntness of a diamond Berkovich indenter is determined based on the results of nanoindentations of half-spaced LiF and KCl samples.

Model equations

We use the mathematical model of a unilateral contact between the Berkovich rigid indenter and an elastic half-space (sample). The indenter with the equation of the surface $x_3 = -f(x_1, x_2)$ is pressed by the force P to a boundary of the contacting sample (see Fig. 1a). The sample is considered as a positive half-space $x_3 \geq 0$. The origin O of Cartesian coordinates, x_1, x_2, and x_3, is put at the single point of the initial contact between the indenter and the sample. The contact region S is an orthogonal projection of the contact between the sample and the lateral surface of the indenter on the plane $x_3 = 0$ after deformation.

Figure 1b demonstrates that the indenter cross-sectional area is not axi-symmetric. The bluntness of the Berkovich indenter is modeled in the same way as in our previous paper [16] in which arcs of different curvature form the surface of the bluntness. All these arcs lie in the planes containing the axis Ox_3. Before deformation, the bottom end of each arc coincides with the origin O in such a way, that the surface of the bluntness is smooth in the vicinity of the origin O. The upper end of each arc lies on the surface of the Berkovich indenter, so that a smooth transition from the blunted shape ($r \leq r_c$) to the pyramidal one ($r > r_c$) occurs. The distance, r_c, is that between the origin, O, and the projection of the upper ends of the arcs to the plane $x_3 = 0$, i.e., r_c defines the contour of the orthogonal projection of the bluntness to the plane $x_3 = 0$. The condition of the smooth transition yields the relations [16]:

$$r_c = R \cdot \cos\gamma, \qquad R = d \cdot \frac{\sin\gamma}{1 - \sin\gamma}, \tag{1}$$

where, R is the radius describing the shape of the blunted indenter, as shown in Fig. 1 and d is the bluntness of the indenter tip. Let us introduce the function $s(M) \equiv s(x_1, x_2) = \frac{\sin\gamma}{1-\sin\gamma}$, where (x_1, x_2) are the coordinates of the point M lying on the plane $x_3 = 0$. Since γ lies in the range [65.3°; 77.05°] (see Fig. 1 in [12]), then $s(x_1, x_2)$ ranges from 9.93 to 38.3, respectively.

The set of NIBEs [13, 14] (with an unknown function $v(M)$, $M \in \Omega$, and displacement h) is applied to formulate the model:

$$\mu v^-(M) + \lambda \iint_\Omega K(M,N) v^+(N) \mathrm{d}S_N = h - f(M), \quad M, N \in \Omega,$$
$$\iint_\Omega v^+(N) \mathrm{d}S_N = P, \mu, \quad \lambda > 0. \tag{2}$$

Here $v^+(M) = \sup\{v(M), 0\}$ is the contact pressure and $v^-(M) = \inf\{v(M), 0\}$. The function $(-\mu v^-(M))$ defines the gap between the indenter and the specimen after deformation and μ is an arbitrary positive parameter. The indenter is rigid, so λ is defined only by the elastic constants of the sample $\lambda = \frac{1-\nu_s^2}{\pi E_s}$. For the region Ω we further assume $\Omega = \{M: h > f(M)\}$. The kernel $K(M, N)$ of the integral operator in (2) accounts for the normal (in the direction Ox_3) and for the tangential (in the plane $x_3 = 0$) displacements of the half-space on the contact surface. If only the blunted shape of the indenter is contacting, then (see (14)):

$$K(M, N) = \frac{1}{R_{MN}} - \frac{\varepsilon}{R} \cdot \frac{x_1^2 + x_2^2 - (x_1\xi + x_2\eta)}{R_{MN}^2} \quad (3)$$

where (x_1, x_2) and (ξ, η) are the coordinates of the points M and N lying on the plane $x_3 = 0$; $2\varepsilon = \frac{1-2\upsilon_s}{1-\upsilon_s}$. The first term in (3) corresponds to the normal displacements of the contact surface. The second one allows for the tangential displacements on the contact surface, which are induced by the surface of the bluntness.

As mentioned in the introduction, we consider the case of shallow indentation, i.e., the contact between the bluntness of an indenter and a sample. This contact occurs if the contact region $S = \{M: v(M) \geq 0\} \subseteq \Omega$ lies within the orthogonal projection of the bluntness to the plane $x_3 = 0$, that is $\{M: v(M) \geq 0\} \subset \{M: r \leq r_c\}$. As follows from Fig. 1, this condition is satisfied if $h < d$. Indeed, let us define r_{contact} as the distance between the origin O and the contour of the contact region S. As is seen from Fig. 1, $r_{\text{contact}} < \sqrt{2hR}$. According to (1) $r_c = R\cos\gamma$. Then, $\frac{r_{\text{contact}}}{r_c} < \frac{\sqrt{2hR}}{R\cos\gamma} = \sqrt{\frac{2h}{d \cdot s(x_1,x_2) \cdot \cos^2\gamma}} \leq \sqrt{\frac{2}{1.92} \cdot \frac{h}{d}} \approx \sqrt{\frac{h}{d}}$.

On the assumption of $r \leq r_c$ one has the following expression for the function $f(M)$:

$$f(M) = R - \sqrt{R^2 - r^2}. \quad (4)$$

However, if $h < d$, then $\left(\frac{r}{R}\right)^2 \ll 1$. Therefore the function in (4) can be approximated as:

$$f(M) = \frac{r^2}{2R}. \quad (5)$$

The function $f(M)$ in (2) and defined further in (5) is not the paraboloid as in the Hertzian problem, since R depends on M accordingly to (1).

Before starting the numerical calculations, the system (2) is reformulated in a dimensionless form (see Appendix B). The derivation of the final formula for the load–displacement diagram:

$$P = \frac{\sqrt{2d}}{\lambda} \cdot P_0(h) \cdot h^{3/2} \quad (6)$$

is also given in Appendix B. To obtain the function $P_0(h)$, the numerical solution of the set in (15) at different values of the mutual approach h is necessary.

Results and discussion

Influence of tangential displacements on the load–displacement curves

The tangential displacements influence the load–displacement curves (6) only via the dimensionless compression force $P_0(h)$. Therefore, it is enough to consider this function to comprehend the relations between tangential displacements and the indentation behavior of different materials.

As can be seen from (15), the equation used for determination of the dimensionless contact pressure U^+ and therefore of $P_0(h)$ includes the displacement h, the parameter of the indenter bluntness d and the Poisson's ratio υ_s of the sample material. Moreover, all these quantities are included only in the term which accounts for tangential displacements. Hence, the influence of the properties of the sample being indented on the value arising tangential displacements is determined by the Poisson's ratio of the sample material υ_s and does not depend on its Young's modulus.

If $\upsilon_s = 0.5$ ($\varepsilon = 0$ for a perfectly incompressible material) then the term accounting for the tangential displacements in (15) is zero and tangential displacements do not arise during indentation. This result is well-known from the literature [17]. In this case the function $P_0(h)$ does not depend on the displacement h. Its value P_0 is determined by the shape of the indenter. The resulting load P in (6) is proportional to $h^{3/2}$.

Otherwise, if $\upsilon_s < 0.5$ ($\varepsilon > 0$), then tangential displacements occur and the relation $\varepsilon \cdot \sqrt{\frac{h}{d}}$ determines their magnitude. The resulting load P is no longer proportional to $h^{3/2}$.

To quantify the effect of tangential displacements on the load-displacement curves, the set (15) was solved numerically and the function $P_0(h)$ obtained at various values of the Poisson's ratio ($\upsilon_s = 0 - 0.5$) of the sample material. The solution for $P_0(h)$ is given in Fig. 2a. The black points correspond to the numerical solutions. Fitting the data set in Fig. 2a by $P_0(h) = P_0 + b \cdot \left(\frac{h}{d}\right)^{\chi}$ yields the curves with parameters that are listed in Table 1.[1] The dimensionless compression force, $P_0(h)$ at $\upsilon_s = 0.5$ is $P_0 = 1.277$ and obtained by the numerical solution of (15). Therefore, the dependences of $P_0(h)$ and $P(h)$ on the displacement h can be approximated by:

$$\begin{aligned} P_0(h) &\approx P_0 + b(\upsilon_s) \cdot \sqrt{\frac{h}{d}}, \\ P(h) &\approx \frac{\sqrt{2d}}{\lambda} \cdot P_0 \cdot h^{3/2} + \frac{\sqrt{2}}{\lambda} \cdot b(\upsilon_s) \cdot h^2, \end{aligned} \quad (7)$$

where $b(\upsilon_s)$ is a function depending on the Poisson's ratio of the sample material, $b(0.5) = 0$.

Parameter λ in the second equation of (7) can be also defined through the reduced Young's modulus E^* [15]:

[1] The dimensionless compression force P_0 is calculated using equation (15). As it is seen, the displacement h and the bluntness d are included in (15) as h/d. Therefore, the solution of (15), P_0, is also a function of h/d.

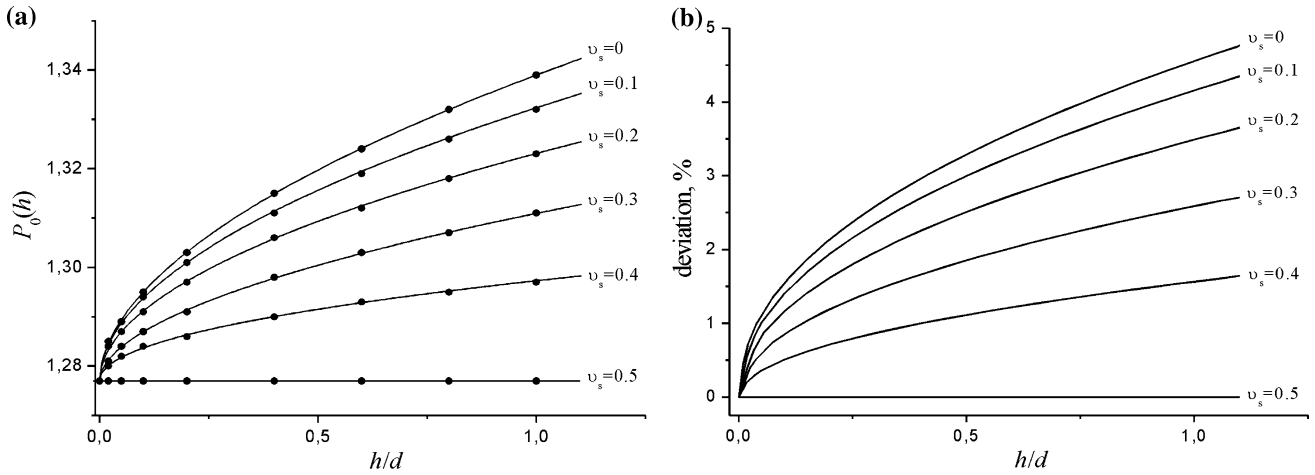

Fig. 2 **a** Dimensionless compression force as a function of the indenter displacement for the samples with different Poisson's ratios. **b** The relative deviation of the load determination, see (8), indicates the influence of the tangential displacements on the determination of the load at a given displacement. The indenter geometry assumed for the numerical simulations is defined by function (5), which coincides with the simulated shape of the blunted indenter at least at $h < d$

Table 1 The values of the parameters b and χ which yield the best-fit of the dimensionless compression force (black points in Fig. 2a) by the function $P_0 + b \cdot \left(h/d\right)^{\chi}$

υ_s	$10^2 \cdot b$	$10 \cdot \chi$
0	6.17 ± 0.08	5.41 ± 0.02
0.1	5.56 ± 0.08	5.37 ± 0.03
0.2	4.63 ± 0.07	5.32 ± 0.03
0.3	3.38 ± 0.05	5.34 ± 0.02
0.4	2.03 ± 0.05	5 ± 0.03
0.5	0	0

$$\lambda = \frac{1}{\pi E^*}, \quad \frac{1}{E^*} = \frac{1-\upsilon_s^2}{E_s} + \frac{1-\upsilon_i^2}{E_i}.$$

Therefore any knowledge concerning E^* are directly applicable in (7). For example, in order to extend (7) to elastically anisotropic solids, one may use approximations of the reduced modulus [18, 19].

It should be noted, that if the tangential displacements in the model are neglected, then the dimensionless compression force is $P_0(h) = P_0 = 1.277$, regardless of the value of Poisson's ratio υ_s. Neglecting tangential displacements one gets smaller values for the dimensionless compression force and consequently a smaller value of the load compared to the values calculated when accounting for tangential displacements. The deviation of the dimensionless compression force (7) is $b(\upsilon_s) \cdot \sqrt{\frac{h}{d}}$ and the deviation of the load (6) is $\Delta P \approx \frac{\sqrt{2}}{\lambda} \cdot b(\upsilon_s) \cdot h^2$. Hence, the load discrepancy growth is approximately quadratic as the displacement increases.

Let us introduce the relative deviation of the load determination $\mathrm{dev} = (P(h) - P_{\mathrm{no\,TD}}(h))/P(h)$, which occurs if tangential displacements are not considered. Accordingly to (7) the relative deviation can be estimated as:

$$\mathrm{dev} = \frac{P(h) - P_{\mathrm{no\,TD}}(h)}{P(h)} \approx \frac{b(\upsilon_s) \cdot \sqrt{\frac{h}{d}}}{1.277 + b(\upsilon_s) \cdot \sqrt{\frac{h}{d}}}, \qquad (8)$$

where $P(h)$ is the load calculated according to (6) with allowance for tangential displacements; $P_{\mathrm{no\,TD}}(h)$ is the load calculated accordingly to (6) with the constant value of $P_0 = 1.277$, i.e., without the allowance for tangential displacements (further the model neglecting tangential displacements). The dependence of the relative deviation function (8) on the dimensionless displacement of the indenter is shown in Fig. 2b for various values of Poisson's ratio υ_s of the sample material. The deviation function grows if the indentation depth increases. Depending on the Poisson's ratio, the relative deviation function can achieve almost 5% at the depth comparable with the value of the parameter of the indenter bluntness.

The influence of the tangential displacements on the solution of (15) can be well demonstrated by a visualization of the profile of the deformed surface of the sample. The profiles represented in Fig. 3a correspond to the cross-section containing Ox_1 and Ox_3, whereas those represented in Fig. 3b correspond to the cross-section containing Ox_2 and Ox_3 (see Fig. 1). To maximize the tangential displacements we applied $\upsilon_s = 0$ in calculations of the profiles. The dashed lines show the profile of the surface before deformation. Figure 3 reveals a considerable incompatibility of strains after deformation (i.e., penetration of elastic half-space into the punch) for the solution ignoring the tangential displacements. However, the

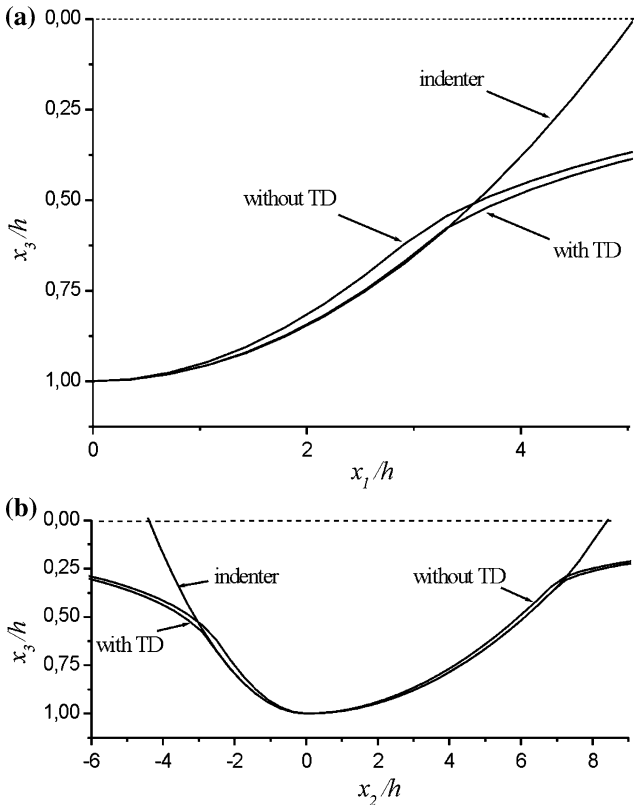

Fig. 3 Profiles of the surfaces of the rigid non-ideal Berkovich indenter and of the deformed elastic half-space at displacement $h = d$. A considerable incompatibility of strains occurs if the formulation of the contact problem (2) omits the tangential displacements ("without TD"). The profile derived applying the solution of the refined contact problem experiences a negligible incompatibility of strains ("with TD"). **a** Cross-section containing Ox_1 and Ox_3. **b** Cross-section containing Ox_2 and Ox_3 (see Fig. 1)

incompatibility of strains significantly decreases, if the solution of (15) accounts for the tangential displacements. As results from (16), tangential displacements reach a maximum value at the boundary of the contact region. If $h = d$, then the maximum value of tangential displacements amounts to 21% of the indentation depth.

Effect of tangential displacements on the nanoindentation study of the reduced Young's modulus

The Oliver–Pharr method is a commonly used technique for processing the nanoindentation data [20, 21]. The reduced Young's modulus is determined from the contact stiffness S and the projected contact area A using the Bulychev–Alekhin–Shorshorov (BAS) relation [15, 20, 22]:

$$S = \frac{2\beta^*}{\sqrt{\pi}} E^* \sqrt{A}$$

where β^* ("*" is applied to distinguish from the indenter parameter β) is a constant that depends on the geometry of the indenter. The BAS relation neglects the tangential displacements. We can derive from the second equation in (7) a refined relation for the contact stiffness S_{TD} that accounts for the tangential displacements:

$$S_{\mathrm{TD}} = \frac{\mathrm{d}P(h)}{\mathrm{d}h} \approx \sqrt{2}\pi E^* \cdot \left(\frac{3}{2} \cdot \sqrt{d} \cdot P_0 \cdot h^{1/2} + 2 \cdot b(\upsilon_s) \cdot h\right). \quad (9)$$

Tangential displacements influence the reduced modulus E^* by means of the contact stiffness only because the contact area is not explicitly presented in (9). The effect of tangential displacements is associated with the second term in (9). Therefore, the contact stiffness that neglects the tangential displacements is:

$$S_{\mathrm{no\,TD}} = \frac{\mathrm{d}P(h)}{\mathrm{d}h} \approx \frac{3}{2}\sqrt{2}\pi E^* \cdot \sqrt{d} \cdot P_0 \cdot h^{1/2}. \quad (10)$$

Let E^*_{TD} denotes the reduced modulus determined with allowance for the tangential displacements (9) and $E^*_{\mathrm{no\,TD}}$ denotes the modulus determined neglecting them (10). Relation between E^*_{TD} and $E^*_{\mathrm{no\,TD}}$ can be found from the comparison of S_{TD} with $S_{\mathrm{no\,TD}}$. The contact stiffness is evaluated at the beginning of unloading $h = h_{\max}$ [20]. We should also account for the final displacement h_{f} after complete unloading [20]. Thus we set $h = h_{\max} - h_{\mathrm{f}}$ to compare the contact stiffness in (9) and (10):

$$\frac{E^*_{\mathrm{TD}}}{E^*_{\mathrm{no\,TD}}} = \frac{\frac{3}{2} \cdot \sqrt{d} \cdot P_0 \cdot (h_{\max} - h_{\mathrm{f}})^{1/2}}{\frac{3}{2} \cdot \sqrt{d} \cdot P_0 \cdot (h_{\max} - h_{\mathrm{f}})^{1/2} + 2 \cdot b(\upsilon_{\mathrm{s}}) \cdot (h_{\max} - h_{\mathrm{f}})} \approx 1 - \frac{4}{3} \cdot \frac{b(\upsilon_{\mathrm{s}})}{P_0} \cdot \sqrt{\frac{h_{\max} - h_{\mathrm{f}}}{d}} \approx 1 - b(\upsilon_{\mathrm{s}}) \cdot \sqrt{\frac{h_{\max} - h_{\mathrm{f}}}{d}}$$

Here we used that $b(\upsilon_s) \ll P_0 = 1.277$. The model is developed for a rigid indenter. Therefore, the effect of tangential displacements on determination of the Young's modulus and of the reduced Young's modulus is the same:

$$\frac{E_{\mathrm{s,TD}}}{E_{\mathrm{s,no\,TD}}} = \frac{E^*_{\mathrm{TD}}}{E^*_{\mathrm{no\,TD}}} \approx 1 - b(\upsilon_{\mathrm{s}}) \cdot \sqrt{\frac{h_{\max} - h_{\mathrm{f}}}{d}}. \quad (11)$$

Furthermore, we investigate the case of shallow indentation, $h_{\max} \approx d$. Therefore if $h_{\mathrm{f}} \ll h_{\max}$ then (11) reduces to:

$$\frac{E_{\mathrm{s,TD}}}{E_{\mathrm{s,no\,TD}}} = \frac{E^*_{\mathrm{TD}}}{E^*_{\mathrm{no\,TD}}} \approx 1 - b(\upsilon_{\mathrm{s}}). \quad (12)$$

As follows from (11) and (12), the models neglecting tangential displacements overestimate the reduced and the Young's modules. For a wide range of materials the error in determination of the elastic modulus is about 4% (see

Table 1). For materials with the Poisson's ratio less than 0.2 the error approaches to 6%.

A difficulty of the Oliver–Pharr method is the estimation of the contact area [22, 23]. To avoid this, we propose to find the unknown parameters (d or $E^* = 1/\pi\lambda$) by fitting the function $P(h)$ in (7) to the elastic part of the indentation curves. Corresponding examples are given below.

Application of the refined model to the analysis of experimental load-displacement curves

A number of numerical simulations are carried out in order to interpret the experimental results on elastic nanoindentation of LiF and KCl single crystals [(001) fresh cleavage planes] by a Berkovich indenter. The goal is to find the parameter of bluntness d of the indenter tip, using both the model accounting for the tangential displacements and the model neglecting them. The nanoindentation measurements were carried out with the same blunted Berkovich diamond indenter using the Nano Indenter-II nanohardness tester (MTS Systems Inc., Oak Ridge, USA). The loading and unloading phases of indentation were carried out under load control. At maximum load, a dwell period of 10 s was imposed before unloading, and another dwell period of 30 s at 80% of unloading, to correct for thermal drift in the system. The Young's modulus of the diamond indenter is 1143 GPa and the Poisson's ratio is 0.072.

The LiF single crystal was manufactured by LOMO (Leningrad Optical-Mechanical Amalgamation), located in St. Petersburg, Russia. The total level of impurities was less than 100 ppm. The KCl single crystal was manufactured at the Institute for Single Crystals at National Academy of Scientists of Ukraine, located in Kharkov. It had less than 1 ppm impurities.

Typical plots of nanoindentation of the LiF and KCl specimens in logarithmic coordinates are shown in Fig. 4. The curves indicate the experimental data. We plot only loading curves, since the nanoindentations are elastic at displacements up to 30 nm ($\log(h) \leq 1.5$), i.e., loading and unloading curves are congruent. As will be seen from the results of the simulations, the condition $h < d$ is satisfied.

For our simulations we have put for LiF the Young's modulus 114 GPa and the Poisson's ratio 0.2. For KCl we have put the Young's modulus 24.1 GPa and the Poisson's ratio 0.29. The condition of the model, $E_s/E_i \ll 1$, is fulfilled for both samples. Hence, the tangential displacements of the diamond indenter can be neglected as compared with those of the samples. The black points in Fig. 4 denote the simulations, which account for tangential displacements (with TD), whereas the open circles correspond to the simulations, which neglect tangential displacements (without TD). The values of the bluntness d corresponding to the simulations are summarized in Table 2.

Fitting of the experimental data shown in Fig. 4 is done as follows. For a given displacement h_i within the interval 0–25 nm, we find such a parameter of the indenter bluntness d_i, that the numerically determined load $P(h_i)$ at $d = d_i$ matches the experimental load at the given displacement h_i with an accuracy higher than 0.5%. In this way, a set of bluntness values is produced each of which corresponds to a certain displacement. For the fitting we use a set of displacements, which cover the interval of displacements 0–25 nm with a step-size of about 2.5 nm. The set of values of the indenter bluntness versus the set of displacements is plotted in Fig. 5. The diagrams do not contradict the fact that the bluntness is a fixed geometric parameter. We simply use the bluntness as a natural fit

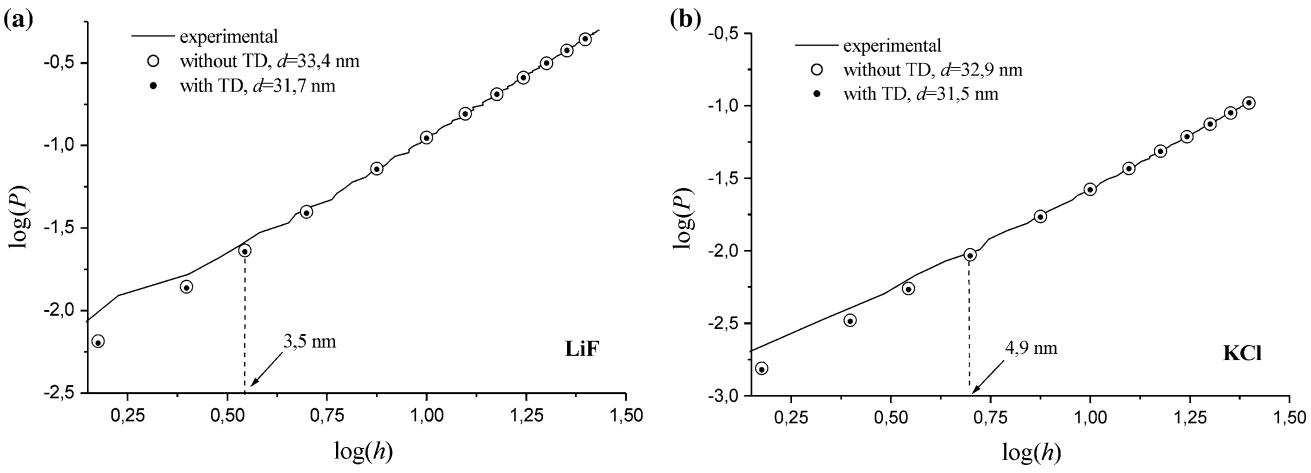

Fig. 4 Load–displacement diagrams for (**a**) LiF and (**b**) KCl in logarithmic coordinates. The curves show the experimental data for elastic indentation. The black points indicate the simulations by means of the refined model whereas the open circles are obtained using the model neglecting tangential displacements

Table 2 The values of the bluntness d of the indenter tip, which are used for the simulations of the experimental load–displacement curves obtained from the nanoindentation of LiF and KCl samples by Berkovich indenter

Sample	d(nm), with TD	d(nm), without TD	Deviation (%)
LiF	31.7	33.4	5.1
KCl	31.5	32.9	4.3

parameter. Figure 5 gives an understanding of how good the models fit the experimental data and whether the models are acceptable for practical implementation. If the models describe the nanoindentation by the blunted indenter realistically, then the evaluated values of the indenter bluntness d_i should be about the same, regardless of displacements. As indicated in Fig. 5, the dependence of evaluated bluntness on displacements is different in two regions: the first one corresponds to displacements smaller than 5 nm (indentation of LiF) or 7.5 nm (indentation of KCl); the second region corresponds to displacements higher than those mentioned above. The evaluated bluntness depends strongly on the displacements in the first region. The value of the bluntness grows abruptly in this region, as displacement decreases. This is the reason, why the simulated load–displacement points do not match the experimental curves in the region of small displacements, as seen in Fig. 4. We suppose that the surface (5) chosen in the models does not properly approximate the geometry of the real indenter tip at small displacements. However, the evaluated bluntness remains approximately constant in the second region, if the model used accounts for tangential displacements (filled circles in Fig. 5). If the model used neglects tangential displacements (open circles in Fig. 5), then the growth of the evaluated bluntness occurs in the second region. This growth is especially evident for KCl, see Fig. 5b. So, the refined model describes nanoindentation qualitatively much better in the second region than the model neglecting them. Comparing to the refined model, the model neglecting tangential displacements yields higher values of the indenter bluntness. The values of the evaluated indenter bluntness averaged over the second region are used for the simulations of the experimental load–displacement curves in Fig. 4. These averaged values are summarized in Table 2.

Influence of tangential displacements on the simulated load–displacement curves is clearly demonstrated in Fig. 6. The curves denote the simulations of nanoindentation of LiF and KCl by the blunted Berkovich indenter by means of the refined model. The values of the bluntness used for the simulations are taken from the column "with TD" in Table 2, with respect to the sample. The open circles correspond to simulations, which neglect tangential displacements. The values of the bluntness used are the same as above. As seen from Fig. 6, by neglecting tangential displacements the simulated values of load are underestimated. The relative deviation of the load determination $\mathrm{dev} = (P(h) - P_{\mathrm{no\,TD}}(h))/P(h)$ is also plotted (dashed).

The diagrams given in Fig. 5 should be constructed for each experiment on elastic nanoindentation in order to determine the limit displacement (like 5–7 nm for the present nanoindentations). The models derived in the paper are valid at displacements larger than the limit displacement. The results at smaller indentations imply that the indenter could be a bit flatter at the tip. To verify this assumption, the bluntness should be approximated by a homogeneous function with the degree higher than 2.

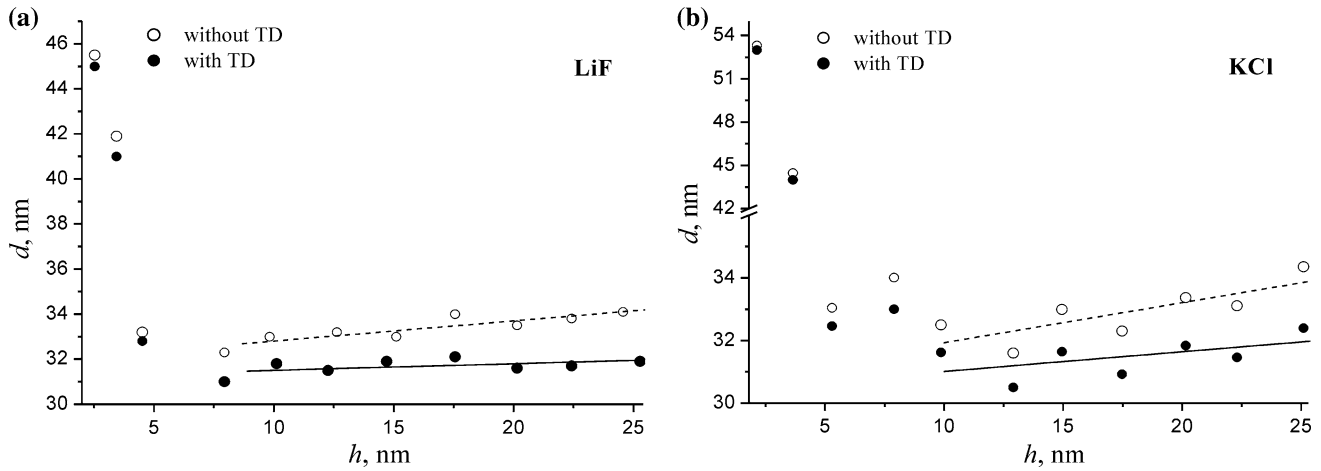

Fig. 5 Determination of the indenter bluntness by the pointwise fitting of the experimental load-displacement curves for (**a**) LiF and (**b**) KCl (see Fig. 4). The filled circles indicate the simulations by means of the refined model whereas the open circles are obtained using the model neglecting tangential displacements

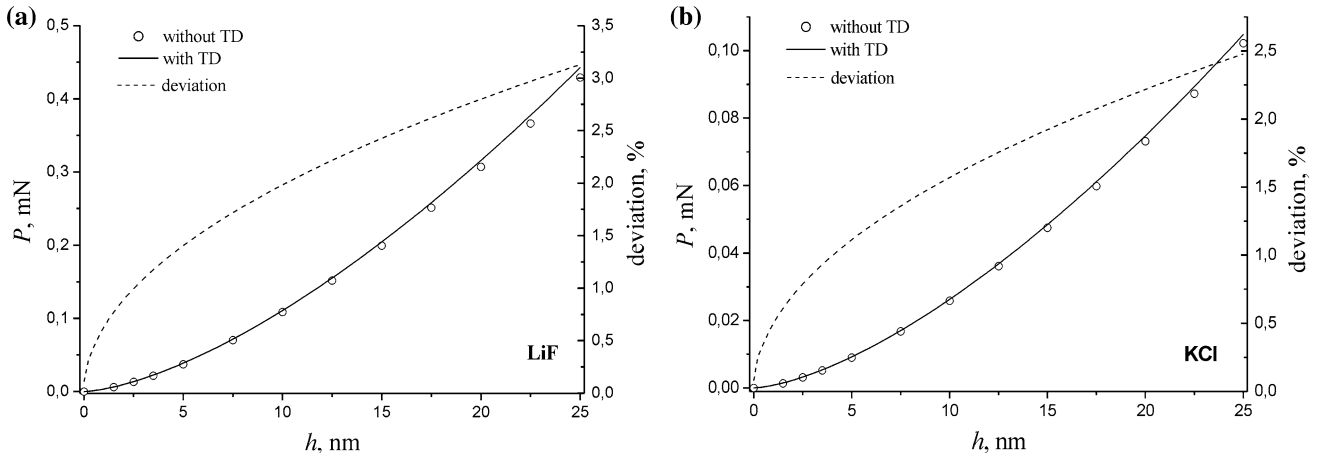

Fig. 6 Simulations of the nanoindentation of (**a**) LiF and (**b**) KCl samples by the blunted Berkovich indenter. The curves are obtained by means of the refined model. The open circles correspond to the model neglecting tangential displacements. Both models assume the same parameter of the indenter bluntness: 31.7 nm for LiF and 31.5 nm for KCl (see Table 2). The relative deviation function is shown as the *dashed curve*

Another possibility to improve predictions of the models at small displacements is the allowance for the local roughness of the indenter. Effect of the roughness on the elastic indentation is given in [17, pp. 419–420]. Johnson defines parameter $\alpha = \sigma/h$, where σ is the standard deviation of surface height distribution: "… the Hertz theory of smooth surfaces can be used with only a few per cent error provided the parameter α is less than about 0.05, …". One could also derive theoretically the influence of parameter α on the contact pressure and on the contact area, like Johnson did for the Hertzian problem. However, it is not necessary, if one can construct diagrams like that in Fig. 5. These diagrams demonstrate that approximation of smooth surfaces is valid at least at displacements larger than the limit displacement. Thus, accounting for the local roughness of the contact surfaces or increasing the degree of the shape function could improve the model for predictions at displacements smaller than the limit displacement. In other words, the limit displacement can be decreased. However, it always exists, because the models derived are the continuum models.

Conclusions

The frictionless shallow indentation of an elastic half-space (sample) by the rigid Berkovich indenter of non-ideal shape is investigated. The formulation does not neglect the tangential surface displacements, coupling them with the normal surface displacements. The derived mathematical model of the elastic contact is based on a set of non-linear integral boundary equations.

The dependence of the load on the indenter displacements consists of two terms. The first term is caused by the normal surface displacements and is proportional to $h^{3/2}$. The second term results from the tangential displacements and is approximately proportional to h^2. This second term vanishes if Poisson's ratio of the sample approaches 0.5. The value of the second term can achieve 5% of the total load, at displacements of the indenter comparable with the value of the parameter of the indenter bluntness. We provide also a simple expression for the impact of the tangential displacements on nanoindentation studies of the reduced Young's modulus.

The model was successfully applied to determine the bluntness parameter of a Berkovich indenter. For this purpose we analyzed the nanoindentation experiments on samples of LiF and KCl produced by this indenter. It was shown that the tangential displacements often ignored could be falsely interpreted as the use of a slightly blunter indenter. The values of the bluntness parameter obtained were different (depending on the investigated sample) if the applied model neglected the tangential displacements. However, the model allowing for the tangential displacements yielded about the same values of the indenter bluntness independent of the measured sample.

Appendix A

Accordingly to [8] the nonlinear boundary integral equation of the contact problem accounting for tangential displacements is:

$$\mu v^-(M)+\lambda\iint\limits_{\Omega}\frac{v^+(N)}{R_{MN}}\mathrm{d}S_N=h-f(x_1+u(M),x_2+w(M)),$$
$$M(x_1,x_2),N(\xi,\eta)\in\Omega. \tag{13}$$

Here $u(M)$ and $w(M)$ are the tangential displacements in point M in the directions Ox_1 and Ox_2 respectively, $v^+(M)$ is the contact pressure. We assume that these displacements are small compared to the dimensions of the contact region. In this case the function $f(x_1+u(M),x_2+w(M))$ from Eq. 13 can be approximated by:

$$\begin{aligned}&f(x_1+u(M),x_2+w(M))\\&\quad=\frac{(x_1+u(M))^2+(x_2+w(M))^2}{2R(x_1+u(M),x_2+w(M))}\\&\quad\approx f(M)+\frac{x_1\cdot u(M)+x_2\cdot w(M)}{R(M)},\end{aligned}$$

where $f(M)$ is defined in (5). We denote further $R(M)$ as R.

The tangential displacements induced by the surface of the bluntness can be introduced as [24]:

$$u(M)=-\lambda\varepsilon\iint\limits_{\Omega}\frac{v^+(N)\cdot(x_1-\xi)}{R_{MN}^2}\mathrm{d}S_N,$$
$$w(M)=-\lambda\varepsilon\iint\limits_{\Omega}\frac{v^+(N)\cdot(x_2-\eta)}{R_{MN}^2}\mathrm{d}S_N.$$

Therefore,

$$\begin{aligned}&f(x_1+u(M),x_2+w(M))\\&\quad\approx f(M)-\frac{\lambda\varepsilon}{R}\iint\limits_{\Omega}\frac{x_1^2+x_2^2-x_1\xi-x_2\eta}{R_{MN}^2}v^+(N)\mathrm{d}S_N.\end{aligned}$$

and Eq (13) allowing for the tangential displacements can be written as

$$\begin{aligned}&\mu v^-(M)+\lambda\iint\limits_{\Omega}\frac{1}{R_{MN}}\\&\quad\times\left[1-\frac{\varepsilon}{R}\cdot\frac{x_1^2+x_2^2-(x_1\xi+x_2\eta)}{R_{MN}}\right]v^+(N)\mathrm{d}S_N\\&\quad=h-f(M),\ M(x_1,x_2),\ N(\xi,\eta)\in\Omega.\end{aligned}\tag{14}$$

In the present formulation of the contact problem the magnitude of the radius R depends on the position of the point M.

Appendix B

Let us formulate the problem (2) in a dimensionless coordinate system $x_{\mathrm{i}}=\sqrt{2hd}x_{0\mathrm{i}}$ and also introduce the dimensionless unknown function $U(x_{01},x_{02})=\lambda\cdot\sqrt{2d/h}\cdot v(x_1,x_2)$. We then write the NBIEs (2) in the following dimensionless form:

$$\begin{aligned}&U^-(M_0)\\&+\iint\limits_{\Omega_0}\frac{1}{R_{M_0N_0}}\\&\quad\left[1-\sqrt{\frac{2h}{d}}\cdot\frac{\varepsilon}{s(x_{01},x_{02})}\cdot\frac{x_{01}^2+x_{02}^2-(x_{01}\xi_0+x_{02}\eta_0)}{R_{M_0N_0}}\right]\cdot\\&\quad U^+(N_0)\mathrm{d}S_{N_0}\\&\quad=1-\frac{x_{01}^2+x_{02}^2}{s(x_{01},x_{02})},\\&\iint\limits_{\Omega_0}U^+(N_0)\mathrm{d}S_{N_0}=P_0(h),\quad M_0,N_0\in\Omega_0,\end{aligned}\tag{15}$$

where M_0 and N_0 are the points on the plane $x_{03}=0$ with the coordinates (x_{01},x_{02}) and (ξ_0,η_0) respectively. $P_0(h)$ is the dimensionless compression force. The square $\Omega_0=\{M_0\colon|x_{01}|\le 6,\ |x_{02}|\le 6\}$ is an image of the square Ω after changing variables. The value 6 is chosen in order that the square Ω_0 includes the contact region $S_0=\{M_0:\ U(M_0)\ge 0\}\subseteq\Omega_0$. Similarly, the dimensionless tangential displacements are given by:

$$u_0(M_0)=-\varepsilon\sqrt{\frac{h}{2d}}\cdot\iint\limits_{\Omega_0}\frac{U^+(N_0)\cdot(x_{01}-\xi_0)}{R_{M_0N_0}^2}\mathrm{d}S_{N_0},$$
$$w_0(M_0)=-\varepsilon\sqrt{\frac{h}{2d}}\cdot\iint\limits_{\Omega_0}\frac{U^+(N_0)\cdot(x_{02}-\eta_0)}{R_{M_0N_0}^2}\mathrm{d}S_{N_0}.\tag{16}$$

The final formula for constructing the $P(h)$ diagram for the approach of the indenter and the sample can be obtained by substituting the second equation in (15) into the second equation in (2)

$$P=\frac{\sqrt{2d}}{\lambda}\cdot P_0(h)\cdot h^{3/2}.\tag{17}$$

The collocation method is used for the discretization of (15). The integrals are approximated by the rectangle formula. To solve the discretized equation the generalized Newton's method is applied.

The region Ω_0 is divided into 1024 equal pieces (i.e. 1089 nodes). Numerical simulations show that the generalized Newton's method converges to the exact solution of the discretized form of the first equation in (15) usually after five iterations at the discrepancy for each node of 1×10^{-5}.

Before starting the numerical simulations, the solution of the NBIEs (15) was compared with that one of the Hertzian problem. For this purpose we assume $s(x_1,x_2)=\mathrm{const}=1$ and $\upsilon_{\mathrm{s}}=0.5$. In this case:

$$P = \frac{\sqrt{2R}}{\lambda} \cdot P_0(h) \cdot h^{3/2}.$$

holds for the compressive force P (see (17)). The solution of the dimensionless NBIEs (15) yields $P_0(h) = \text{const} = 0.3 \pm 2 \cdot 10^{-4}$. Let us compare with the Hertzian problem [17, 24]:

$$P = \frac{2\sqrt{2}}{3\pi} \cdot \frac{\sqrt{2R}}{\lambda} \cdot h^{3/2},$$

where $\frac{2\sqrt{2}}{3\pi} \approx 0.30011$.

References

1. Hertz H (1882) J Reine Angew Math 92:156
2. Galanov BA (1982) Dokl Akad Nauk Ukr SSR 7:36
3. Galanov BA, Grigor'ev ON (1986) Strength Mater 18:1330
4. Brock LM (1979) Int J Eng Sci 17:365
5. Georgiadis HG (1998) Comput Mech 21:347
6. Soldatenkov IA (1994) Mekh Tverd Tela 4:51
7. Soldatenkov IA (1996) J Appl Math Mech 60:261
8. Galanov BA (1983) Mekh Tverd Tela 6:56
9. Argatov II (2004) J Appl Mech Tech Phys 45:118
10. Argatov II (2004) Dokl Phys 49:222
11. Herrmann K, Jennett NM, Wegener W et al (2000) Thin Solid Films 377:394
12. Borodich FM, Keer LM, Korach CS (2003) Nanotechnology 14:803
13. Galanov BA (1993) J Math Sci 66:2414
14. Galanov BA (1985) J Appl Math Mech 49:634
15. Borodich FM, Keer LM (2004) Int J Solids Struct 41:2479
16. Kindrachuk VM, Galanov BA, Kartuzov VV et al (2006) Nanotechnology 17:1104
17. Johnson KL (1985) Contact mechanics. Cambridge University Press, Cambridge
18. Vlassak JJ, Nix WD (1994) J Mech Phys Solids 42:1223
19. Vlassak JJ, Ciavarella M, Barber JR et al (2003) J Mech Phys Solids 51:1701
20. Pharr GM, Oliver WC, Brotzen FR (1992) J Mater Res 7:613
21. Mencik J (2007) Meccanica 42:19
22. Oliver WC, Pharr GM (2004) J Mater Res 19:3
23. Khan MK, Hainsworth SV, Fitzpatrick ME et al (2009) J Mater Sci 44:1006. doi:10.1007/s10853-008-3222-9
24. Landau LD, Lifshitz EM (1986) Theory of elasticity. Pergamon Press, New York